J Mater Sci (2009) 44:5364–5374
DOI 10.1007/s10853-009-3514-8

FERROELECTRICS

Compositionally graded ferroelectric multilayers for frequency agile tunable devices

C. V. Weiss · M. B. Okatan · S. P. Alpay · M. W. Cole · E. Ngo · R. C. Toonen

Received: 23 March 2009 / Accepted: 22 April 2009 / Published online: 8 May 2009

Abstract Recently, there has been significant interest toward the development of tunable dielectric materials for voltage-controlled, frequency-agile phase shifters and filters operating in the microwave regime. The fundamental challenge in designing materials systems for such tunable devices is the simultaneous requirement of high dielectric tunability (>40%) over a large temperature interval (−10 °C to +90 °C) coupled with low dielectric losses (between 3.0 dB and 4.0 dB in operational bandwidths ranging from several hundred MHz up to 30 or more GHz). We show that a high- and temperature-insensitive tunability can be realized in compositionally graded ferroelectrics and provide a brief review of the results of experimental and theoretical studies on the dielectric properties of Barium Strontium Titanate ($Ba_{1-x}Sr_xTiO_3$ or BST) multilayer heterostructures. Theoretically, we discuss the role of thermal stresses on the dielectric properties using a non-linear thermodynamic model coupled with basic electrostatic considerations to describe the interlayer interactions between the ferroelectric layers. We show that the thermal strains arising from the thermal expansion coefficient mismatch between the multilayered film and the substrate may have a significant effect on the dielectric permittivity and tunability of BST multilayers. Experimentally, compositionally graded BST multilayers (5 mol% MgO doped and undoped) were grown via metallo-organic solution deposition (MOSD) on Pt–Si substrates and electrically characterized. Optimum conditions were found to exist in BST multilayers consisting of three distinct layers of ~220 nm nominal thickness with compositions corresponding to $Ba_{0.60}Sr_{0.40}TiO_3$ (BST 60/40), BST 75/25, and BST 90/10. At room temperature, the BST heterostructure has a small-signal dielectric permittivity of 360 with a dissipation factor of 0.012 and a dielectric tunability of 65% at 444 kV/cm. These properties exhibit minimal dispersion as a function of temperature ranging from 90 °C to −10 °C. Our results also show that MgO doping improves dielectric loss ($\tan\delta = 0.008$), but results in a moderate dielectric tunability of 29% at 444 kV/cm. Electrical measurements at microwave frequencies display a decrease in the dielectric permittivity and tunability for both undoped and MgO-doped BST multilayers. At 10 GHz, the dielectric response, tunability, and the loss characteristics for graded undoped BST are 261, 25% (at 1,778 kV/cm), and 0.078, respectively, and 189 and 15% (at 1,778 kV/cm), and 0.039, respectively, for the MgO-doped graded BST.

C. V. Weiss · M. B. Okatan · S. P. Alpay (✉)
Materials Science and Engineering Program and Institute of Materials Science, University of Connecticut, Storrs, CT 06269, USA
e-mail: p.alpay@ims.uconn.edu

M. W. Cole · E. Ngo · R. C. Toonen
Weapons and Materials Research Directorate, Active Materials Research Group, U.S. Army Research Laboratory, Aberdeen Proving Ground, MD 21005, USA

M. W. Cole
e-mail: mcole@arl.army.mil

Introduction

Non-linear dielectric materials are promising candidates for use in a variety of tunable devices, such as phase shifters, tunable filters, delay lines, and oscillators because the dielectric response of the material can be adjusted or "tuned" with the application of an external electric field [1, 2]. Ferroelectric (FE) materials are well-known for their strong non-linear response to an applied electric field, both

in the paraelectric and ferroelectric states. In the FE state, in addition to the non-linear response, the polarization also displays hysteretic behavior due to polarization switching. Therefore, research for materials to be used in tunable devices has focused on FE materials in their paraelectric state. One of the leading material candidates for tunable ferroelectrics is Barium Strontium Titanate ($Ba_{1-x}Sr_xTiO_3$ or BST). In BST, the phase transition temperature or the Curie temperature (T_C) which indicates the onset of ferroelectric behavior can be adjusted by varying the relative amounts of barium and strontium content. The T_C for pure barium titanate ($BaTiO_3$, BTO) is $\sim$120 °C, but by adding strontium titanate ($SrTiO_3$, STO) to make the solid solution BST, T_C can be decreased [3]. For example, $Ba_{0.70}Sr_{0.30}TiO_3$ (BST 70/30) has a T_C of $\sim$34 °C and for BST 60/40 $T_C \approx 5$ °C [4–8]. The ability to tailor T_C by controlling the composition is one of the most promising aspects of using BST in different types of tunable electronic devices [9] since the dielectric permittivity and tunability can be maximized in the vicinity of the FE to paraelectric phase transformation. There are several comprehensive reviews on tunable materials, loss mechanisms, device configurations, and specifically BST thin films for tunable device applications [2, 9, 10].

Although BST is a very promising material system to be employed in tunable devices, many limitations of the materials still exist. In order to be utilized in tunable devices, a material must have a high tunability (typically above 40%), a low loss tangent, temperature stability, and all of these properties must be maintained in the microwave range of frequencies (300 MHz to 300 GHz) [11–13]. Furthermore, the high dielectric response and tunability of bulk or single-crystal BST cannot be realized in thin film form, mainly due to the internal strains that arise in thin film systems. These strains are caused by many factors, including the lattice mismatch between the film and substrate if the films are epitaxial, the difference in coefficients of thermal expansion (CTE) for the film and substrate, the self-strain of the FE phase transformation if the material is grown above the phase transformation temperature, and "microstrains" due to defects such as dislocations and vacancies [14, 15]. For example, the relative dielectric constant for bulk BST 70/30 can be greater than 10,000 near T_C, while a BST film (thickness $\sim$200 nm) of the same composition is predicted to have a dielectric constant of about 300 near T_C [16].

In addition to the internal stresses, the dielectric properties such as tunability and loss are also highly temperature dependent in BST thin films. Temperature stability is crucial for the application of BST in tunable devices for telecommunication applications because these systems will be operated in a large range of temperatures (typically −10 °C to 90 °C). Recently, much research has been devoted to graded FE films to control the strains in the thin film structure and consequently improve the dielectric properties and temperature stability. Our theoretical results indicate that the tunability of graded multilayer FEs can then be maximized by optimizing the internal electric fields that arise between layers due to the polarization mismatch [17]. Depending on the internal stress state and the magnitude of the in-plane strains, such heterostructures may also display relatively temperature insensitive dielectric response and tunability.

Although many FE materials may exhibit high tunabilities, the dielectric loss is still quite high for use in many types of microwave tunable devices. One method that has been identified to improve the loss of these materials is through acceptor doping. Dopants (such as Ni^{2+}, Al^{2+}, Ga^{3+}, $Mn^{2+,3+}$, $Fe^{2+,3+}$, Mg^{2+}, etc.) typically occupy the B-site of the ABO_3 perovskite structure, substituting for Ti^{4+} ions. The charge difference between the dopant and the Ti^{4+} atom can effectively compensate for oxygen vacancies and may decrease dielectric losses [18, 19]. For example, dielectric constant, loss tangent, and tunability (at 237 kV/cm) of BST 60/40 for 5 mol% MgO-doped BST 60/40 thin films were reported as 720, 0.1, 28%, and 334, 0.007, 17.2%, respectively [20]. Among all the doping elements used with BST and other ferroelectric materials, MgO has been identified as one of the most promising candidate for lowering the loss, and thus we will focus on the effect of MgO addition to the dielectric tunability [20, 21].

Since compositionally graded FE films can improve the dielectric response of the thin film over a large temperature range and acceptor doping has been shown to lower dielectric loss, MgO doping combined with compositionally graded FE multilayers presents an opportunity to enhance material properties for tunable devices that require a high tunability, low loss, and temperature insensitivity. In this article, we summarize the findings of our recent theoretical and experimental work that incorporates the abovementioned approaches to improve the dielectric properties of BST thin films. The next section contains a thermodynamic model that provides quantitative results for graded BST tri-layers as a function of the CTE difference between the multilayer heterostructure and the substrate. We calculate the dielectric properties and tunability of such multilayers as a function of the CTE of the substrate, the processing temperature, the applied electric field, and the operation temperature. The "Experimental: multilayer films" section concentrates on the deposition of graded BST multilayer films, microstructural characterization, and measurement of the dielectric properties. In the "Experimental: MgO-doped multilayer films" section, we discuss the role of acceptor doping and graded films on the dielectric response and tunability of multilayer BST films at microwave frequencies.

Thermodynamic theory of graded multilayer FE films: thermal stresses

Understanding the role of internal stresses on the functional properties of FE thin films is crucial to tailor the material properties for different tunable device requirements. It is now well understood that the substrate-induced in-plane strain has a strong influence on the ultimate phase stability of a FE film. Particularly in the case of epitaxial, single-crystalline systems, recent developments demonstrate that it is possible to create FE phases that may not be found in the single-crystal or bulk parent compound under ambient conditions. Examples include strain-induced ferroelectricity at room temperature in the "incipient" FE STO [22], strain-induced ferroelectricity at room temperature of BST 60/40 thin films with Strontium Ruthenate ($SrRuO_3$ or SRO) electrodes [23], and rotational phases in ultra-thin $PbTiO_3$ (PTO) [24]. These observations are supported by theoretical studies that predict unconventional phases under large mechanical strains, in particular, for in-plane tensile strains. Studies show that compressive strains (in the plane of the film-substrate interface) may enhance the tetragonal out-of-plane polarization [25, 26], while in-plane tensile strains induce in-plane rotational phases of the polarization. [24] These developments have been reviewed recently by Schlom et al. [27]. Furthermore, FE films may also exhibit a complex defect microstructure, which may include features such as twins (or poly-domains) [28], in-plane atomic ordering [29], interfacial misfit dislocations (MDs) [30], and threading dislocations (TDs) [31–34]. The evolution of this complicated microstructure is in direct response to the internal stresses that develop during film growth and subsequent cooling from the deposition and processing temperatures.

Since all the films and heterostructures have to be processed at elevated temperatures (typically 500–800 °C), the CTE mismatch between the film and the substrate becomes a significant parameter that may by itself have a tremendous impact on the dielectric properties [35]. The strain state in the case of a multilayered FE heterostructure or a graded FE film is also inhomogeneous [36]; a position-dependent internal in-plane strain arises from thermal stresses resulting from cooling down from the deposition temperature or the annealing temperature. The reference temperature that determines the thermal strain depends on what is chosen as the processing technique. For physical vapor deposition methods such as pulsed laser deposition (PLD), the critical temperature is the temperature of the substrate during deposition (T_G). For chemical deposition techniques such as spin coating, dip-coating, or metallo-organic chemical vapor deposition (MOCVD), the temperature of interest is the final annealing temperature (T_A). It is therefore crucial to understand the degree by which the thermal strains alter the dielectric response and its tunability.

We begin our analysis by assuming a [001]-textured (along the z-direction, see schematic drawing in Fig. 1) BST film consisting of n compositionally distinct layers. This texture is chosen to isolate the effects of the thermal strains from strain arising from lattice mismatch. The free energy density of each layer in its bulk form can be expressed through a Landau expansion of the form:

$$F(P,T) = F_0 + \frac{1}{2}aP^2 + \frac{1}{4}bP^4 + \frac{1}{6}cP^6 \quad (1)$$

where F_0 is the free energy density of the reference polarization-free paraelectric state above T_C, P is the polarization, and a, b, and c are the dielectric stiffness coefficients. The temperature dependence of the coefficient a is given by the Curie-Weiss law such that $a = (T - T_C)/\varepsilon_0 C$, where ε_0 is the permittivity of free space, and T_C and C are the Curie temperature and constant, respectively.

In the case of a thin film of a FE clamped by a thick substrate, there exists a biaxial in-plane stress due to the thermal stresses that arise as the material is cooled down from a processing temperature T_A. Considering the mechanical boundary conditions (equal in-plane stresses and the film being traction-free in the z-direction), a straightforward Legendre transformation results in renormalized Landau coefficients. Using these boundary conditions and the short-circuit conditions illustrated in Fig. 1, the free energy functional for a multilayered FE film as a function of thermal stresses becomes [37]

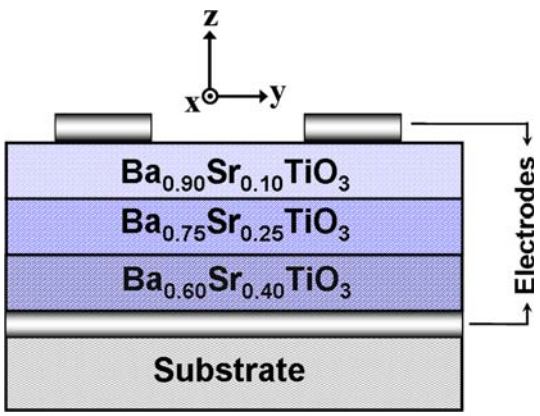

Fig. 1 Schematic diagram of the graded trilayer BST thin film, including a view of the top and bottom electrodes

$$F_\Sigma = \sum_{i=1}^{n} \alpha_i \left[F_{0,i} + \frac{1}{2} a_i' P_i^2 + \frac{1}{4} b_i' P_i^4 + \frac{1}{6} c_i P_i^6 - E^{\text{ext}} P_i + \frac{x_i^2}{s_{11,i} + s_{12,i}} \right] - \frac{1}{2} \sum_{i=1}^{n} \alpha_i E_{D,i} P_i \quad (2)$$

in which

$$a_i' = a_i - x_i \frac{4Q_{12,i}}{s_{11,i} + s_{12,i}} \quad (3)$$

$$b_i' = b_i + \frac{4Q_{12,i}^2}{s_{11,i} + s_{12,i}} \quad (4)$$

$$x_i = \int_{T_A}^{T_f} (\lambda_S - \lambda_i) \mathrm{d}T \quad (5)$$

$$\sum_{i=1}^{n} \alpha_i E_{D,i} P_i = -\frac{1}{\varepsilon_0} \sum_{i=1}^{n} \alpha_i (1 - \alpha_i) P_i^2 + \frac{2}{\varepsilon_0} \sum_{i=1}^{n-1} \left[\alpha_i P_i \left(\sum_{j=i+1}^{n} \alpha_j P_j \right) \right] \quad (6)$$

where α_i is the volume fraction of layer i. $Q_{mn,i}$ and $s_{mn,i}$ are the electrostrictive coefficients and elastic compliances of layer i, respectively. x_i is the thermal strain in layer i that results from cooling from a high processing temperature T_A to the operation temperature T_f, due to the mismatch between the CTEs (λ) of the substrate and layer i. E^{ext} is the externally applied electric field. The electrostatic interlayer interaction is established through the depolarizing fields $E_{D,i}$ in layers i that follows from the short-circuit conditions:

$$\sum_{i=1}^{n} \ell_i E_{D,i} = 0 \qquad i = 1, 2, \ldots, n \quad (7)$$

$$(P_i - P_{i+1}) + \varepsilon_0 (E_{D,i} - E_{D,i+1}) = 0 \quad i = 1, 2, \ldots, (n-1) \quad (8)$$

where ℓ_i is the thickness of layer i. The above set of relations yield the depolarizing field in each layer as:

$$E_{D,i} = -\frac{1}{\varepsilon_0} \left(P_i - \sum_{j=1}^{n} \alpha_j P_j \right) \quad (9)$$

where

$$\alpha_i = \frac{\ell_i}{\sum_k^n \ell_k}. \quad (10)$$

The equilibrium polarizations in the individual FE layers (P_i) follow from the simultaneous solution of the equations of state, $\partial F_\Sigma / \partial P_i = 0$. This results in a system of equations for the layers $i = 1, 2, \ldots, n$ given by:

$$\alpha_i \left[a_i P_i + b_i P_i^3 + c_i P_i^5 - \frac{4Q_{12,i}}{s_{11,i} + s_{12,i}} P_i x_i - Q_{12,i} P_i^2 + \frac{1}{\varepsilon_0} \left(P_i - \sum_{j=1}^{n} \alpha_j P_j \right) - E^{\text{ext}} \right] = 0 \quad (11)$$

Following the calculation of P_i, the relative small-signal average dielectric response of a perfectly insulating multilayer can be determined from

$$\langle \varepsilon \rangle \cong \frac{1}{\varepsilon_0} \frac{\mathrm{d}\langle P \rangle}{\mathrm{d}E} \quad (12)$$

where

$$\langle P \rangle = \sum_{i}^{n} \alpha_i P_i \quad (13)$$

is the average polarization. The dielectric tunability of the multilayer heterostructure at a particular temperature, T, can then be calculated as the change in the average dielectric constant at an applied electric field, E^{ext}, with respect to the average dielectric constant at zero applied field;

$$\%\eta = \frac{(\langle \varepsilon \rangle @ E = 0\,\text{V/m}, T) - (\langle \varepsilon \rangle @ E, T)}{(\langle \varepsilon \rangle @ E = 0\ \text{V/m}, T)} \times 100 \quad (14)$$

For the numerical analysis, we consider a trilayer-graded BST heterostructure as shown in Fig 1. It consists of three layers of equal thickness with compositions corresponding to $Ba_{0.90}Sr_{0.10}TiO_3$ (BST 90/10), BST 75/25, and BST 60/40. We assume that in each layer the thermodynamic parameters (the Curie temperature, Curie constant, dielectric stiffness coefficients, electrostrictive coefficients, elastic compliances, and CTEs) are a linear function of the composition and may be determined by averaging the corresponding values for BTO and STO [4, 5, 22]. CTEs of each layer were assumed to be independent of temperature.

First, we examine the average polarization at room temperature of the trilayer BST structure as a function of the CTE of the substrate and the annealing temperature. Our results show that there is the same trend for all the annealing temperatures in the range of 550–750 °C; below a certain CTE value ($\sim 10.2 \times 10^{-6}\ \text{K}^{-1}$), the BST multilayer is not spontaneously polarized [37]. In other words, the large in-plane stresses that develop in cooling from a high annealing temperature suppress ferroelectric behavior on substrates with a CTE less than this critical value. These substrates include STO, lanthanum aluminate ($LaAlO_3$, LAO), and sapphire (α-Al_2O_3). It is also important to note that if the CTE of the trilayer BST is less than that of the substrate, there are in-plane compressive strains that balance the additional contributions to the free energy from

the electrostatic field due to the (initial) polarization mismatch between the compositional layers [37]. In this case, therefore, the multilayer is expected to exhibit spontaneous polarization, and thus ferroelectricity.

Figure 2a and b plot the calculated average dielectric permittivity at room temperature (RT = 25 °C) of the BST multilayer at an applied electric field of 0 kV/cm and 400 kV/cm, respectively. The corresponding dielectric tunability is plotted in Fig. 2c. The average dielectric permittivity decreases monotonically above and below the critical CTE value of the substrate. For a particular CTE at $E^{ext} = 0$, the (small-signal) dielectric response increases as the annealing temperature is lowered. On the other hand, when an external electric field of 400 kV/cm is applied, the permittivity increases with increasing annealing temperature for films under biaxial tensile stresses and decreases with increasing annealing temperature for films under biaxial compressive stresses. In Fig. 2c, the tunability of the BST multilayer film is shown; it exhibits a maximum that is close to 100% at the critical CTE value of the substrate. The tunability increases as the annealing temperature is lowered for both stress states below and above the critical CTE.

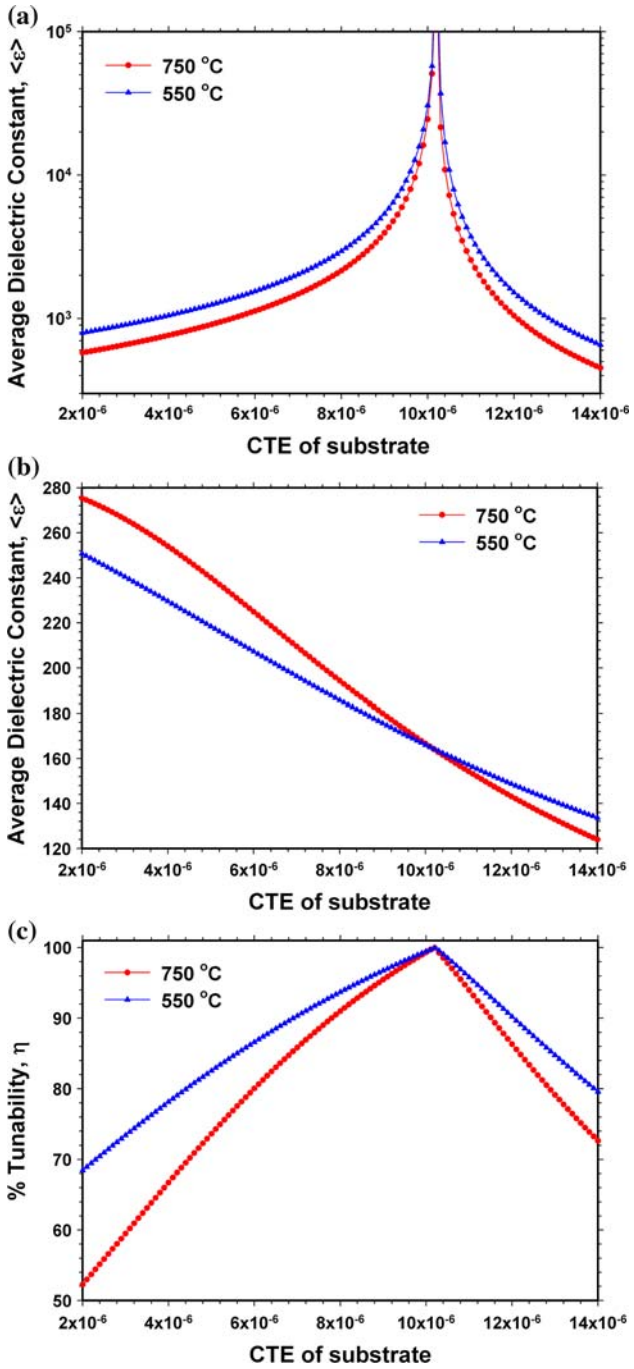

Fig. 2 Dielectric constant of the BST trilayer at **a** $E = 0$ kV/cm and **b** $E = 400$ kV/cm; **c** tunability of the BST trilayer at $E = 400$ kV/cm

In Fig. 3, we show a three-dimensional (3D) plot to demonstrate the effect of varying the temperature and the applied electric field on the tunability of the trilayer BST film deposited on Si with $T_A = 750$ °C. As the electric field is increased at a given temperature, the tunability increases reaching a value of ~65% at an applied electric field of 400 kV/cm, measured at room temperature (20 °C). The tunability can be further increased by lowering the temperature, with a maximum tunability of ~75% at −50 °C and a field of 400 kV/cm. Overall, we note that by decreasing the temperature and increasing the applied field, the tunability can be increased significantly. However, this also indicates that the tunability of such trilayer BST devices will be lower at smaller applied fields (which are desired to minimize power usage) and higher temperatures (including those temperatures where tunable devices operate). Future work in this field will undoubtedly focus on maintaining a high tunability (and simultaneous low loss) at lower applied fields, high temperatures, and at microwave frequencies, which will be discussed in the final section.

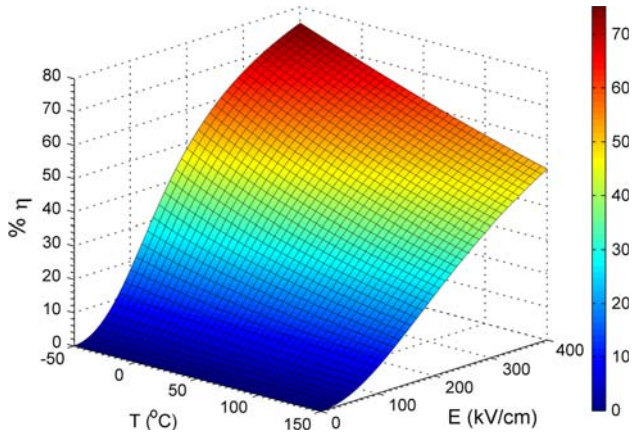

Fig. 3 A 3D plot showing the tunability of the trilayer BST thin film as a function of the temperature, T and the applied electric field, E on a Si substrate ($T_A = 750$ °C)

Experimental: multilayer films

BST is currently fabricated through a variety of techniques, including sputtering [38], PLD [39], sol–gel [40], polymeric precursor methods [41], and others. Metallo-organic solution deposition (MOSD) can produce extremely uniform films since the mixing occurs at the molecular level. The MOSD is also an affordable technique for depositing on large-area substrates with precise control of the stoichiometry and viscosity of the BST precursor solution. Multilayered BST thin films were fabricated via MOSD using barium acetate, strontium acetate, and titanium isopropoxide as the precursor materials and glacial acetic acid and 2-methoxyethanol as the solvents. First, barium acetate and strontium acetate were dissolved in glacial acetic acid, and the solution was stirred for 1 h until it was clear. Then, the titanium isopropoxide was dissolved in 2-methoxyethanol, and this was added to the barium/strontium solution. The solution was stirred for an additional hour. The precursor solution was spin-coated onto Pt–Si substrates, and particulates were removed from the solution using 0.2-μm syringe filters. 2-methoxyethanol was added to the solution as needed to adjust the viscosity (and hence the thickness of each spun-on layer) [21, 42]. After the deposition of each layer, the films were pyrolyzed on a hot plate at 350 °C for 10 min in air to remove any organic addenda. This process was repeated until films of approximately ~225-nm thickness were produced. After the deposition of each compositional layer, the films were annealed at 750 °C for 1 h in flowing oxygen. This "multi-anneal" protocol was used because it has been shown that this annealing procedure helps to minimize the interdiffusion that would take place between the layers if only one annealing step was used [43]. Although a low annealing temperature is beneficial in terms of reducing the thermal stresses, BST thin films processed at 750 °C have been shown to have high-quality crystalline microstructure [43]. The films consist of three compositional layers of BST: BST60/40, BST75/25, and BST90/10, as shown in Fig. 1 and described in the theoretical framework. A uniform composition film of the same thickness, corresponding to BST60/40 was also fabricated to compare the effect of the multilayers on the microstructure and dielectric properties. The thin films were characterized by X-ray diffraction (XRD), field emission scanning electron microscopy (FESEM), atomic force microscopy (AFM), and dielectric/electrical measurements.

Since the theoretical results indicate that a higher processing temperature often degrades the dielectric properties due to the large thermal strains, we choose the lowest annealing temperature that fully crystallizes the BST and produces a well-formed, defect-free microstructure (750 °C). In "Thermodynamic theory of graded multilayer fe films: thermal stresses" section, the importance of the CTE mismatch of the substrate and the BST film was demonstrated, and it was found to play a significant role in determining the dielectric properties. In the experimental synthesis, we used Si substrates. Although the CTE mismatch between Si and BST layers is relatively large ($\sim 7 \times 10^{-6}$ K^{-1} for BST60/40 and Si at room temperature) [37], metallized Si is required as a substrate so that the tunable device is compatible with the existing integrated circuit (IC) technology. While other substrates may produce better dielectric properties, Si was chosen partly because of its affordability and compatibility with current microelectronic systems. Much of this research in the field of FE thin films focuses on optimizing and integrating other substrates into the IC architecture, and it will likely be focus of future research as well.

A cross-sectional FESEM image is given in Fig. 4. This image demonstrates that the films possess a dense, randomly oriented, polycrystalline microstructure with a thickness of ~225 nm. We also note that there is a clear delineation between the bottom Pt electrode and the BST film, promoting good contact properties. Furthermore, the FESEM image shows that there are no visible "interface regions" between the BST layers of different composition.

The AFM micrographs are given in Fig. 5. The AFM micrographs verify that the films have a dense polycrystalline structure with no observable pinholes or other surface defects. In addition to obtaining AFM images, we also measured the roughness of the BST films. Low surface roughness is crucial if the films are to be integrated in devices, because an overly rough surface can cause bad contact between the film and top electrode and this promotes high conductor loss. A smooth film (roughness $<\sim 5$ nm) promotes better contact properties between the film and electrode, thereby lowering the leakage current and overall insertion loss and providing long-term reliability in the device structure. The roughness of the

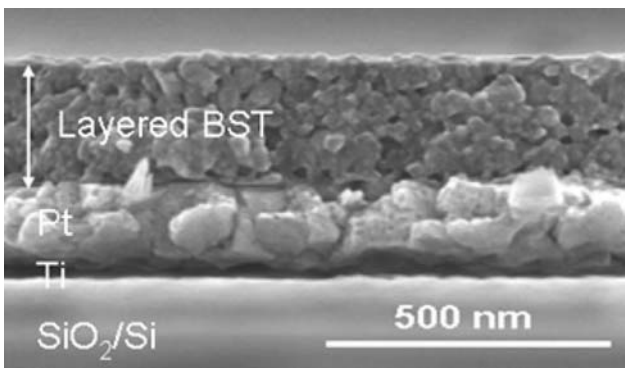

Fig. 4 Cross-sectional FESEM image showing the undoped trilayer BST thin film on the Pt–Si substrate (Reprinted with permission from American Institute of Physics, Copyright 2007)

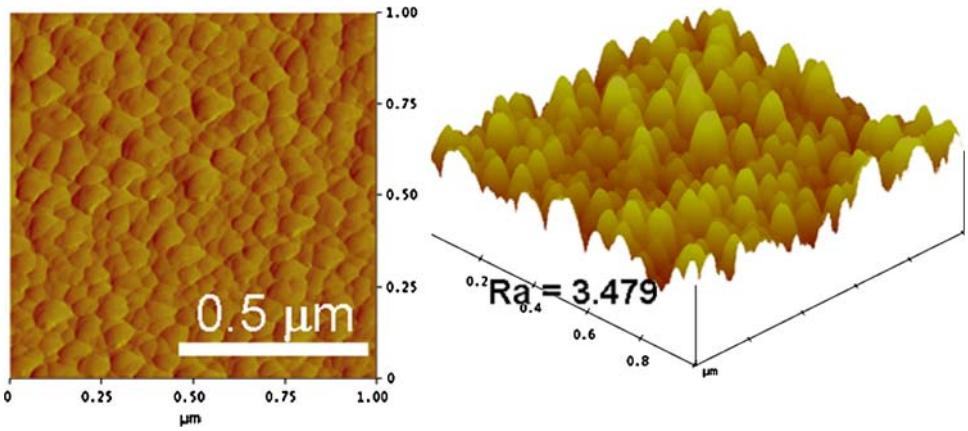

Fig. 5 Plan-view and cross-sectional AFM images of the undoped trilayer BST thin film, demonstrating the dense grain structure and low surface roughness (Reprinted with permission from American Institute of Physics, Copyright 2007)

multilayer films was found to be ~3.5 nm, which is well within the acceptable range for tunable devices. This surface roughness value is comparable to roughness values found in uniform film BST thin films fabricated by the same method.

X-ray diffraction results are given in Fig. 6. In general, the XRD data confirm that the films have a polycrystalline perovskite structure (of the form ABO_3). No secondary phases are present in the film. In comparing the XRD data for the uniform BST60/40 film and the graded (or "up-graded," designated by "UG") BST film, we see a slight downshift in peak positions for the graded film. The downshift may be attributed to the larger lattice parameter in the multilayer films, which is caused by the increase in lattice parameter as the Ba/Sr ratio increases. Since the lattice parameter of the multilayer film is an average of the lattice parameters of each of the layers, the increasing Ba/Sr ratio in the film causes a larger average lattice parameter, and hence the XRD peak shifts downward [43]. The increase in lattice parameter may also arise from the cooling of the films from a high annealing temperature, since interface defects and thermal strains may develop in the film as it is cooled, as described earlier. In fact, the strain field in these BST films is highly non-uniform (as mentioned previously), and may be due to a number of factors, including the variation in the lattice parameter with thickness, localized strains due to defects, and interface regions [42, 44, 45].

Dielectric measurements were carried out using an HP4194A impedance/gain analyzer as well as an in-house temperature measurement station, including a thermoelectric heating stage, inert N_2 ambience, and automated control via a computer system. As discussed in the theoretical model, multilayer films should be temperature insensitive due to the polarization mismatch between the compositionally distinct BST layers. The dielectric permittivity and loss tangent as a function of temperature are given in Fig. 7, confirming the theoretical prediction that permittivity and loss tangent values are stable over the

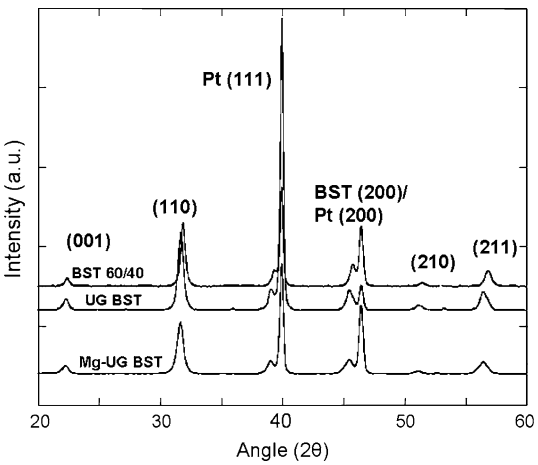

Fig. 6 X-ray diffraction patterns of the uniform BST60/40 film (top), the multilayer "up-graded" BST film (middle), and the MgO-doped multilayer film (bottom) (Reprinted with permission from American Institute of Physics, Copyright 2008)

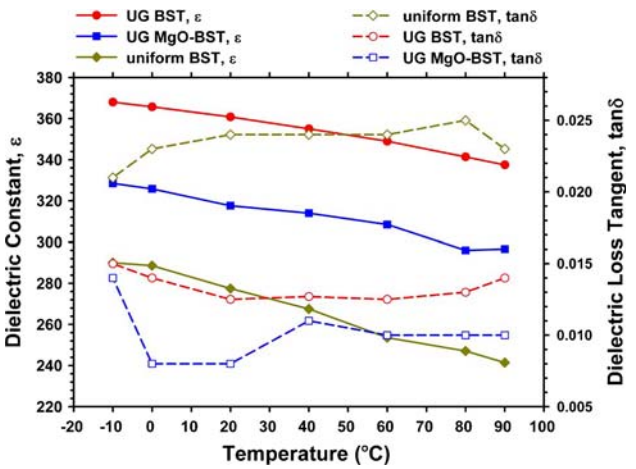

Fig. 7 The dielectric constant and loss tangent of uniform composition BST, undoped multilayer upgraded (UG) BST films, and MgO-doped multilayer UG BST films as a function of temperature (Reprinted with permission from American Institute of Physics, Copyright 2008)

temperature range of −10 °C to 90 °C in the multilayer construct. There is no evidence of anomalous peaks, which often indicate the phase transition temperature of one of the multilayer compositions [39]. The multilayer BST film possessed both a higher permittivity ($\varepsilon = 364$) and lower loss ($\tan\ \delta = 0.012$) then the uniform BST60/40 films ($\varepsilon = 280$ and $\tan\ \delta = 0.023$) at room temperature. Although the composition BST60/40 has a Curie temperature just below room temperature (5 °C), making it paraelectric at room temperature, the compositions of BST75/25 and BST90/10 have different T_C values as discussed earlier, and they have higher permittivity values which increase the average dielectric response for the multilayer film construct. Also, higher permittivity in the multilayer films may be influenced by the electrostatic reaction between different compositional layers. Figure 7 also verifies the theoretical results given in Fig. 3, mainly that in the graded multilayer films, the dielectric response increased as the temperature decreased. Overall though, the multilayer structure produced mostly temperature insensitive behavior in the range −10 °C to 90 °C, as predicted by the thermodynamic model.

The loss tangent for the multilayer film is lower then the uniform composition film, and it is also quite low compared to many results in the literature, including graded films made by sol–gel, PLD, and other methods [39, 46]. However, dielectric loss values for graded BST thin films span a large range in the experimental literature, most likely due to the differences in crystalline quality, defect concentration, and thermal and mechanical strains that arise during thin film deposition and processing [47, 48]. Although the increase in permittivity values in multilayered films can be attributed to the presence of ferroelectric layers and interlayer electrostatic coupling, the lower loss values in multilayered films is not as well understood. The lower loss tangent in multilayered films may be due to the fact that defects are "trapped" at the compositional interfaces and are no longer mobile enough to reach the electrodes and contribute to the loss mechanism.

The tunability of the multilayered BST compared to the uniform BST thin film is given in Fig. 8. Here, we see an increase of ∼56% in the tunability for the trilayer film as compared to the uniform composition BST thin film, due to the increase in the permittivity in the multilayer film as discussed above.

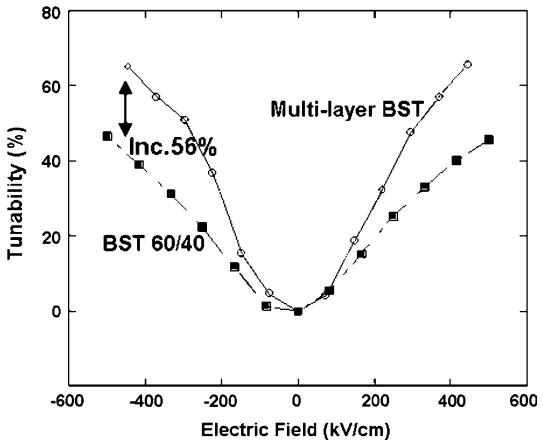

Fig. 8 Tunability at room temperature of the uniform BST60/40 film (filled squares) and the trilayer BST thin film (open circles) as a function of the applied electric field (Reprinted with permission from American Institute of Physics, Copyright 2007)

Experimental: MgO-doped multilayer films

Doping BST films with MgO has been determined as one of the ways to lower the loss tangent. Therefore, combining acceptor doping with a multilayered film design can help lower loss, while simultaneously maintaining a high permittivity and tunability over a wide temperature range. The same experimental procedure and device design described above were used to make the BST films, except that in this case, each compositional layer is MgO-doped BST. We will compare the doped multilayered films to that of an undoped multilayer BST film, and a uniform composition BST60/40 film.

As in the case for the undoped multilayer films, XRD, AFM, and FESEM results indicate that the film has a dense, well-crystallized microstructure with randomly oriented grains and no defects or secondary phases. Compared to some other experimental results involving MgO-doping of BST, our XRD results indicates an enhanced degree of solubility of the MgO. This enhanced solubility is most likely due to the mixing at the molecular level that occurs in the MOSD process, as well as the induced thermal strains discussed previously [49]. Here, we chose 5 mol% MgO doping because it has been shown that a concentration in excess of 10 mol% creates a film that is no longer single phase [21]. In addition to the increase in lattice parameter that was observed in the multilayer structure, we also get an additional increase in the lattice parameter due to the MgO doping. Since Mg has a larger ionic radius that Ti (0.072 nm compared to 0.061 nm), the addition of MgO into the lattice actually causes the lattice to expand slightly, which we can observe in the XRD data in Fig. 6. The AFM micrographs indicate that the doping of BST with MgO produced a smaller grain size (60 nm vs. 72 nm for the undoped multilayer film). This smaller grain size caused a decrease in the overall surface roughness as well (3.1 nm vs. 3.5 nm for the undoped multilayer film). Overall, MgO doping of multilayer films causes enhanced material properties, such as lower surface roughness, and maintains the desirable microstructure for BST in tunable devices.

Figure 7 shows the permittivity and loss for the MgO-doped multilayered films as a function of temperature. We see that the permittivity and loss are both very stable as a function of temperature from −10 °C to 90 °C, as expected from the graded multilayer film design. The doped, multilayer film has a lower loss than the undoped multilayer film (0.010 at 90 °C compared to 0.014 for the undoped multilayer film at 90 °C), but the MgO-doped film also has a lower dielectric constant (330 at −10 °C compared to 370 for the undoped multilayer film at −10 °C). Even though the MgO-doped graded film has a lower permittivity, the low loss and temperature stability are promising results for the use of MgO doping and compositional grading in temperature-stable tunable devices.

Since the doped multilayer films have been shown to possess very low loss (due to the MgO doping) and exceptional temperature stability (due to the compositional grading), we now will examine the dielectric properties (permittivity, loss, and tunability) as a function of frequency. Many tunable devices will be operated in the microwave range of frequencies, but we expect that the dielectric properties will degrade at very large frequencies due to relaxation effects caused by the presence of defects [50]. Therefore, we compare the permittivity, loss, and tunability of the undoped and doped multilayer films at three frequencies: 0.5 GHz, 5 GHz, and 10 GHz. We expect the MgO doping to have a strong influence on the loss characteristics of the multilayer film at high frequencies; however, it is important to note that the permittivity (and hence the tunability, given by Eq. 13), is closely related to the loss tangent. For example, even though acceptor doping has been shown to decrease loss in BST thin films, it has also been shown to decrease the permittivity and tunability. In determining the best film characteristics (such as the "strength" of the compositional gradient, the number of compositional layers, the dopant material, and the doping concentration), we must keep in mind that the simultaneous requirement of low loss and high tunability will ultimately represent a compromise between these two parameters [12].

Figure 9 shows the variation in the permittivity with the applied field for (a) the trilayer BST film and for (b) the MgO-doped trilayer BST film at microwave frequencies. As expected, doping with MgO lowers the permittivity of the trilayer structure at all the applied frequencies. This phenomena can be partly explained by the fact that adding MgO lowers T_C [51]. Also, adding MgO into the BST lattice causes a slight volumetric expansion, as discussed previously [52]. However, we note that as the frequency is increased, the permittivity values are fairly constant for the doped film, whereas in the undoped film, the frequency has a large effect on the permittivity. Therefore, we expect that acceptor doping might prove to be a useful method to maintain a nearly constant dielectric response over a large range of frequencies, including microwave frequencies.

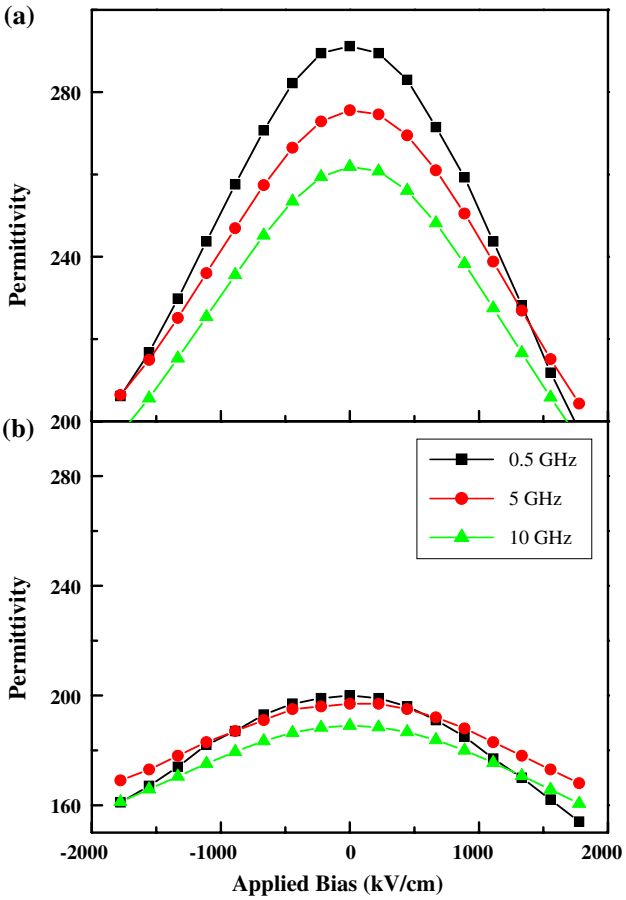

Fig. 9 The permittivity of **a** the undoped multilayer BST film and **b** the MgO-doped multilayer BST film at 0.5, 5, and 10 GHz frequencies (Reprinted with permission from American Institute of Physics, Copyright 2008)

In Fig. 10, we have plotted the loss as a function of the applied field for the undoped (a) and doped (b) graded multilayer films. For both films, we see that increasing the frequency causes an increase in the loss tangent. This increase in the dielectric loss is most likely due to a number of effects, including quasi-Debye type losses, and losses associated with oxygen vacancies and other defects [12]. However, this increase in the loss is much more pronounced in the undoped film, confirming our prediction that doping the trilayer structure with MgO would lower losses at microwave frequencies. Although the loss at microwave frequencies is significantly higher than at lower frequencies (0.008 at 100 kHz for the undoped trilayer film, compared to 0.039 at 10 GHz for the doped, trilayer film [52]), these loss values are still within the acceptable range for many types of tunable devices.

Figure 11 shows tunability as a function of the applied electric field for (a) an undoped trilayer BST film and (b)

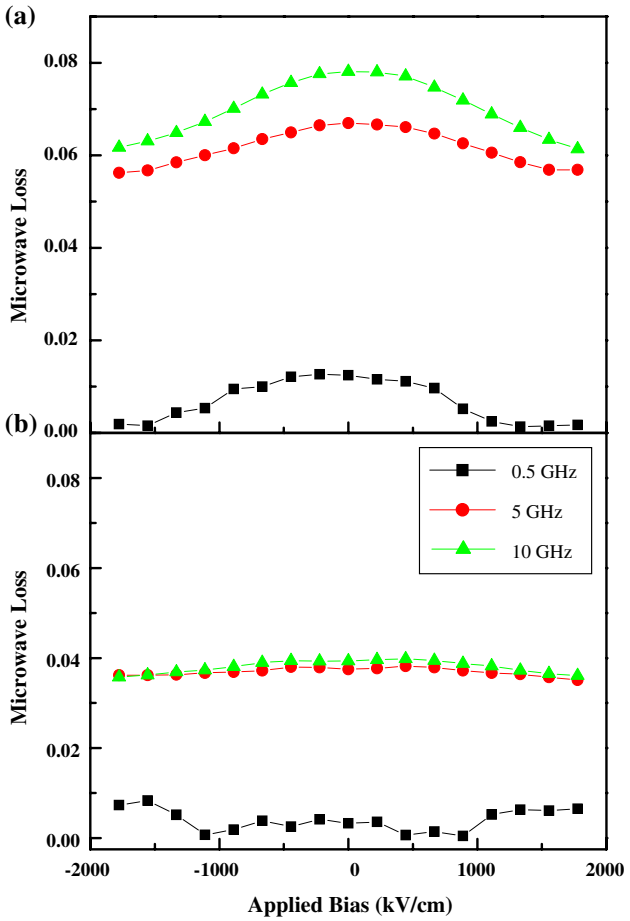

Fig. 10 The microwave dielectric loss tangent of **a** the undoped multilayer BST film and **b** the MgO-doped multilayer BST film at 0.5, 5, and 10 GHz (Reprinted with permission from American Institute of Physics, Copyright 2008)

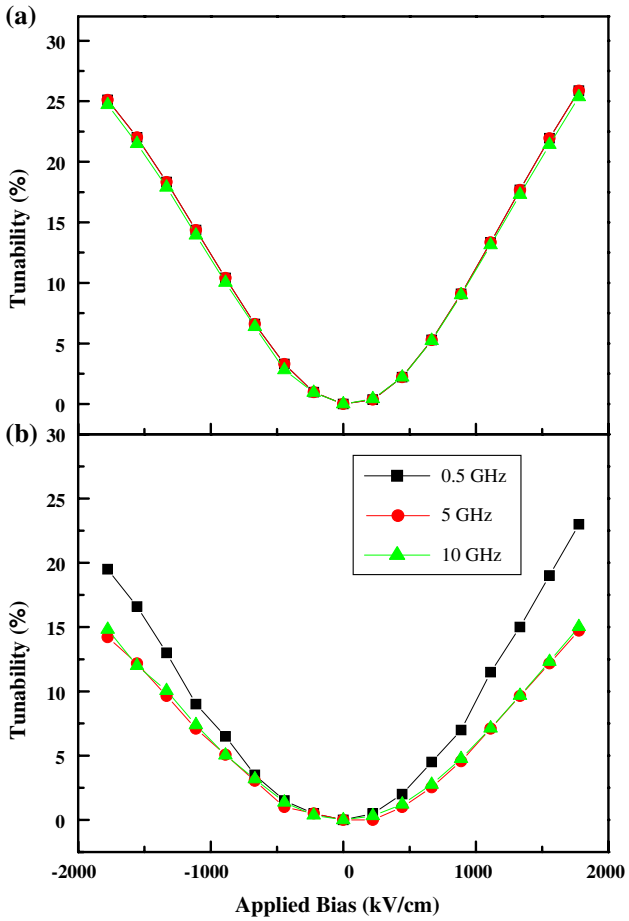

Fig. 11 The tunability of **a** the undoped multilayer BST film and **b** the MgO-doped multilayer BST film measured at 0.5, 5, and 10 GHz (Reprinted with permission from American Institute of Physics, Copyright 2008)

and MgO-doped trilayer BST film. Doping with MgO lowered the tunability, which is related to the decrease in the permittivity discussed above. The MgO doping also caused a larger dispersion in tunability with applied frequency, as compared to the undoped film. For example, the tunability of the MgO-doped graded multilayer film at 1,778 kV/cm and 10 GHz is 15%, while at the same applied field and 0.5 GHz, the tunability is 20%. For the undoped trilayer film, the tunability did not show a significant change with the frequency.

Although compositional grading and acceptor doping have demonstrated excellent dielectric properties into the microwave range of frequencies, many other methods to improve the dielectric properties of ferroelectric thin films over a large frequency and temperature range are currently being investigated. Some of the methods currently being investigated include choosing the appropriate substrate [53] and carefully adjusting the thin film thickness [54]. The theoretical results also indicate that dielectric properties can be improved over a wide temperature and frequency range by finding a substrate with the appropriate CTE, tailoring the multilayer structure, and adjusting the processing temperature. All the three of these approaches were found to affect the strain state in the thin film, which in turn has a profound effect on the dielectric properties of permittivity, loss, and tunability.

Conclusions

The main obstacles to integrating BST thin films into tunable devices are the temperature dependence of their dielectric properties and their relatively large dielectric loss values (especially at microwave frequencies). In order to improve the dielectric response of BST thin films over a wide range of temperatures and frequencies, we examined here the effect of using compositionally graded BST multilayers. Theoretical results based on a non-linear thermodynamic model indicate that the thermal strains arising from the CTE mismatch between the film and substrate

significantly influence the dielectric permittivity and tunability of BST multilayers. Experimentally, BST compositionally multilayered (5 mol% MgO-doped and undoped) films were fabricated via MOSD on Pt–Si. The best dielectric properties (dielectric permittivity of 360, loss of 0.012, and a tunability of 65% at 444 kV/cm) were found to exist in BST heterostructures consisting of three distinct layers of ~220 nm nominal thickness with compositions corresponding to BST 60/40, BST 75/25, and BST 90/10. These properties exhibited minimal dispersion as a function of temperature ranging from 90 °C to −10 °C. Although MgO doping improves dielectric loss, it also results in a moderate tunability (29% at 444 kV/cm). Electrical measurements at 10 GHz display a decrease in the dielectric permittivity and tunability for both undoped and MgO-doped BST multilayers.

Acknowledgements This study at UConn was supported by the U.S. Army Research Office through Grants W911NF-05-1-0528 and W911NF-08-C-0124. The authors would like to thank C. Hubbard for the XRD measurements, and S. Hirsch for the SEM analysis.

References

1. Lancaster MJ, Powell J, Porch A (1998) Supercond Sci Tech 11:1323
2. Tagantsev AK, Sherman VO, Astafiev KF, Venkatesh J, Setter N (2003) J Electroceram 11:5
3. Kingery WD, Bowen HK, Uhlmann DR (1976) Introduction to ceramics, 2nd edn. Wiley, New York
4. Pertsev NA, Zembilgotov AG, Tagantsev AK (1998) Phys Rev Lett 80:1988
5. Pertsev NA, Tagantsev AK, Setter N (2000) Phys Rev B 61:R825
6. Landolt H, Bornstein R (1981) Numerical data and functional relationships in science and technology. Springer, Berlin
7. Yamada T (1972) J Appl Phys 43:328
8. Hilton AD, Ricketts BW (1996) J Phys D: Appl Phys 29:1321
9. Bao P, Jackson TJ, Wang X, Lancaster MJ (2008) J Phys D: Appl Phys 41:1
10. Vendik OG, Hollmann EK, Kozyrev AB, Prudan AM (1999) J Supercond 12:325
11. Wu L, Wu S, Chang FC, Shen YT, Chen YC (2000) J Mater Sci 35:5945. doi:10.1023/A:1026722206381
12. Cole MW, Weiss CV, Ngo E, Hirsch S, Coryell LA, Alpay SP (2008) Appl Phys Lett 92:182906
13. Cole MW, Hubbard C, Ngo E, Ervin M, Wood M, Geyer RG (2002) J Appl Phys 92:475
14. Ban ZG, Alpay SP (2002) J Appl Phys 91:9288
15. Ban ZG, Alpay SP (2003) J Appl Phys 93:504
16. Shaw TM, Suo Z, Huang M, Liniger E, Laibowitz RB, Baniecki JD (1999) Appl Phys Lett 75:2129
17. Zhong S, Alpay SP, Mantese JV (2006) Appl Phys Lett 88:132904
18. Cole MW, Joshi PC, Ervin MH (2001) J Appl Phys 89:6336
19. Podpirka A, Cole MW, Ramanathan S (2008) Appl Phys Lett 92:212906
20. Cole MW, Nothwang WD, Hubbard C, Ngo E, Ervin MH (2003) J Appl Phys 93:9218
21. Cole MW, Joshi PC, Ervin MH, Wood MC, Pfeffer RL (2000) Thin Solid Films 374:34
22. Li YL, Choudhury S, Haeni JH, Biegalski MD, Vasudevarao A, Sharan A, Ma HZ, Levy J, Gopalan V, Trolier-McKinstry S, Schlom DG, Jia QX, Chen LQ (2006) Phys Rev B 73:184112
23. Qin WF, Ai WY, Zhu J, Xiong J, Tang JL, Zhang Y, Li YR (2007) J Mater Sci 42:8707. doi:10.1007/s10853-007-1739-y
24. Catalan G, Janssens A, Rispens G, Csiszar S, Seeck O, Rijnders G, Blank DHA, Noheda B (2006) Phys Rev Lett 96:127602
25. Roytburd AL, Alpay SP, Nagarajan V, Ganpule CS, Aggarwal S, Williams ED, Ramesh R (2000) Phys Rev Lett 85:190
26. Ederer C, Spaldin NA (2005) Phys Rev Lett 95:257601
27. Schlom DG, Chen LQ, Eom CB, Rabe KM, Streiffer SK, Triscone JM (2007) Ann Rev Mater Res 37:589
28. Kwak BS, Erbil A, Budai JD, Chisholm MF, Boatner LA, Wilkens BJ (1994) Phys Rev B 49:14865
29. Zhang LC, Vasiliev AL, Misirlioglu IB, Ramesh R, Alpay SP, Aindow M (2008) Appl Phys Lett 93:262903
30. Speck JS, Daykin AC, Seifert A, Romanov AE, Pompe W (1995) J Appl Phys 78:1696
31. Misirlioglu IB, Vasiliev AL, Alpay SP, Aindow M, Ramesh R (2006) J Mater Sci 41:697. doi:10.1007/s10853-006-6488-9
32. Misirlioglu IB, Alpay SP, Aindow M, Nagarajan V (2006) Appl Phys Lett 88:102906
33. Misirlioglu IB, Vasiliev AL, Aindow M, Alpay SP, Ramesh R (2004) Appl Phys Lett 84:1742
34. Vrejoiu I, Le Rhun G, Zakharov ND, Hesse D, Pintilie L, Alexe M (2006) Philos Mag 86:4477
35. Sharma A, Ban ZG, Alpay SP, Mantese JV (2004) Appl Phys Lett 85:985
36. Akcay G, Zhong S, Allimi BS, Alpay SP, Mantese JV (2007) Appl Phys Lett 91:012904
37. Okatan MB, Cole MW, Alpay SP (2008) J Appl Phys 104:104107
38. Tsai MS, Sun SC, Tseng TY (1997) J Appl Phys 82:3482
39. Lu SG, Zhu XH, Mak CL, Wong KH, Chan HLW, Choy CL (2003) Appl Phys Lett 82:2877
40. Jain M, Majumder SB, Katiyar RS, Miranda FA, Van Keuls FW (2003) Appl Phys Lett 82:1911
41. Saravanan KV, Raju KCJ, Krishna MG, Bhatnagar AK (2007) J Mater Sci 42:1149. doi:10.1007/s10853-006-1435-3
42. Zhu X, Lu S, Chan HLW, Choy CL, Wong KH (2003) Appl Phys A: Mater Sci Process 76:225
43. Cole MW, Ngo E, Hirsch S, Demaree JD, Zhong S, Alpay SP (2007) J Appl Phys 102:034104
44. Jiang Q, Gao YH, Cao HX (2004) Phys Lett A 331:117
45. Tian HY, Luo WG, Pu XH, Qiu PS, He XY, Ding AL (2001) Solid State Commun 117:315
46. Zhu X, Chan HLW, Choy CL, Wong KH (2002) J Vac Sci Tech A: Vac Surf Films 20:1796
47. Zhu XH, Chong N, Chan HLW, Choy CL, Wong KH, Liu Z, Ming N (2002) Appl Phys Lett 80:3376
48. Kim WJ, Chang W, Qadri SB, Pond JM, Kirchoefer SW, Chrisey DB, Horwitz JS (2000) Appl Phys Lett 76:1185
49. Okhay O, Wu AY, Vilarinho PM (2005) J Eur Ceram Soc 25:3079
50. Elissalde C, Ravez J (2001) J Mater Chem 11:1957
51. Su B, Button TW (2004) J Appl Phys 95:1382
52. Cole MW, Ngo E, Hirsch S, Okatan MB, Alpay SP (2008) Appl Phys Lett 92:072906
53. Su B, Button TW, Price T, Iddles D, Cannell D (2008) J Mater Sci 43:847. doi:10.1007/s10853-007-2216-3
54. Weiss CV, Cole MW, Alpay SP, Ngo E, Toonen RC, Hirsch SG, Demaree JD, Hubbard C (2008) Integr Ferroelectr 100:36